
This is an electronic reprint of the original article.
This reprint may differ from the original in pagination and typographic detail.

Meng, Yang; Majoinen, Johanna; Zhao, Bin; Rojas Gaona, Orlando

Form-stable phase change materials from mesoporous balsa after selective removal of lignin

Published in:
Composites Part B: Engineering

DOI:
[10.1016/j.compositesb.2020.108296](https://doi.org/10.1016/j.compositesb.2020.108296)

Published: 15/10/2020

Document Version
Peer-reviewed accepted author manuscript, also known as Final accepted manuscript or Post-print

Published under the following license:
CC BY-NC-ND

Please cite the original version:
Meng, Y., Majoinen, J., Zhao, B., & Rojas Gaona, O. (2020). Form-stable phase change materials from mesoporous balsa after selective removal of lignin. *Composites Part B: Engineering*, 199, Article 108296. <https://doi.org/10.1016/j.compositesb.2020.108296>

Journal Pre-proof

Form-stable phase change materials from mesoporous balsa after selective removal of lignin

Yang Meng, Johanna Majoinen, Bin Zhao, Orlando J. Rojas



PII: S1359-8368(20)33346-1

DOI: <https://doi.org/10.1016/j.compositesb.2020.108296>

Reference: JCOMB 108296

To appear in: *Composites Part B*

Received Date: 21 February 2020

Revised Date: 15 July 2020

Accepted Date: 23 July 2020

Please cite this article as: Meng Y, Majoinen J, Zhao B, Rojas OJ, Form-stable phase change materials from mesoporous balsa after selective removal of lignin, *Composites Part B* (2020), doi: <https://doi.org/10.1016/j.compositesb.2020.108296>.

This is a PDF file of an article that has undergone enhancements after acceptance, such as the addition of a cover page and metadata, and formatting for readability, but it is not yet the definitive version of record. This version will undergo additional copyediting, typesetting and review before it is published in its final form, but we are providing this version to give early visibility of the article. Please note that, during the production process, errors may be discovered which could affect the content, and all legal disclaimers that apply to the journal pertain.

© 2020 Published by Elsevier Ltd.

Yang Meng and Orlando J. Rojas: Conceptualization, Methodology. **Yang Meng and Orlando J. Rojas:** Writing. **Johanna Majoinen:** Writing Support. **Yang Meng:** Visualization, Investigation. **Orlando J. Rojas:** Supervision. **Bin Zhao:** Experimental support. **Yang Meng, Johanna Majoinen, Orlando J. Rojas:** Writing- Reviewing and Editing,

Form-Stable Phase Change Materials from Mesoporous Balsa after Selective Removal of Lignin

Yang Meng^{1,2}, Johanna Majoinen¹, Bin Zhao¹, Orlando J. Rojas^{1,3,*}

¹ Department of Bioproducts and Biosystems, School of Chemical Engineering, Aalto University, P.O. Box 16300, FIN-00076 Aalto, Espoo, Finland.

² College of Materials Science and Technology, Beijing Forestry University, No.35, Qinghua East Road, Haidian District, Beijing, 100083, P.R. China.

³ Departments of Chemical & Biological Engineering, Chemistry and, Wood Science, 2360 East Mall, The University of British Columbia, Vancouver, BC V6T 1Z3, Canada.

*Author for correspondence: Orlando J. Rojas, Email: orlando.rojas@ubc.ca; Tel. +16048223457

ABSTRACT

We produce balsa-based structures by selective removal of lignin. The changes that occur in the main components of balsa upon delignification, including tracheids, closed pits and tylosis vessels, allow the development of mesopores and a substantial increase in fluid permeability. Such system is ideally suited as a support of phase change materials, PCM. Vacuum-assisted impregnation with polyethylene glycol (PEG, a PCM), results in a form-stable PCM system (FPCM). The FPCM displays a high encapsulating capacity (83.5 %) at temperatures above the melting PEG transition, with a latent heat of 134 J/g and low supercooling (12 °C). The results are

rationalized by the affinity between the unidirectional mesoporous structure and the polymer, involving capillary forces and hydrogen bonding. The leakage-proof FPCM outperforms available systems (based on PEG or other PCMs) supported on minerals or other wood species. Compared to the latter group, the results obtained with balsa relate with its morphology and the effect of residual hemicelluloses in hierarchically-aligned cellulose nano- and microfibrils. The FPCMs resist compressive loads and performs stably for at least 200 cycles of heating and cooling. An insignificant loss in latent heat is observed compared to that of pure PEG. The phase transition temperature fluctuation and non-leaking characteristics under load make the balsa-based FPCM a superior alternative for passive heating/cooling, especially for uses at high ambient temperatures. The reversible thermoregulatory capacity, low cost, high efficiency, renewability, and operability of the balsa-supported FPCM, indicate an excellent option for thermal energy storage and conversion devices.

Keywords: Form-stable phase change material; thermal energy storage; balsa; cooling; heating.

1. Introduction

The growing concerns of climate change make affordable materials for efficient energy conversion and management more relevant than ever [1,2]. As such, thermal energy storage materials (TESMs) based on sensible, latent and chemical heat, have emerged as promising solutions to cope with imbalances between energy supply and demand [3]. Among the TESMs, phase change materials (PCMs) capable of storing, transporting, and converting latent thermal energy through phase transition, present an attractive combination of isothermal latent heat, high energy storage density, and chemical stability [4,5]. Up to now, various types of PCMs have been investigated for solar energy conversion and storage [6,7], for waste heat recovery devices [8], intelligent temperature-responsive sensors [9], reversible thermochromic building [10], Li-ion

batteries thermal management [11], tunable luminescent materials [12], infra-red stealth [13], and thermo-regulated smart textiles [14].

Due to the lower degree of supercooling and excellent thermal stability, organic PCMs are often considered for TESMs [15,16]. An example is polyethylene glycol (PEG), especially given its high latent enthalpy, biocompatibility, low vapor pressure, low cost, easy modification, adjustable phase transition temperature, non-corrosiveness, and non-toxicity [17]. However, like other organic PCMs (such as fatty acids, fatty alcohols, and paraffin), the transition from solid-to-liquid phases makes PEG handling challenging, mainly, because of the fluidity and leakage when supported by solids. PEG confinement in a supporting material has been proposed as a solution [18], for example, earlier efforts in this direction considered metallic hollow substrates. However, the associated high cost as well as low metal thermal conductivity have restricted related developments [19]. Recent reports indicate encapsulation with porous scaffolds toward form-stable composite phase change materials (FPCMs) that are easily adaptable in devices [20]. So far, lightweight natural clay minerals, including diatomite [21], halloysite [22], and vermiculite [23] have been used as PEG-based FPCMs. However, the thermal storage capability of these powder-based FPCMs is $< 60\%$ for PEG, failing to meet the demands for efficiently harvesting or releasing thermal energy. Three-dimensional (3D) porous scaffolds comprising carbon sponges, ceramic foams, and graphene aerogels have been proposed for their relatively high thermal energy storage capacity [24]. However, the needed “bottom-up” fabrication strategies, including layer-by-layer assembly of nano- or micro-scale materials (carbon nanotubes [25], graphene nanoplatelets [26], and boron nitride whiskers [27]), are tedious and result in inhomogeneous porous structures, with disconnected capillarity. In addition, toxic organic additives are often required, increasing the environment load. Thus, effective and sustainable 3D porous scaffolds that are easy to manufacture and with sustained performance remain highly desirable.

Responding to the above needs, living plants have brought a new perspective. For instance, wood comprises a highly aligned natural structures comprising hollow vessels and tracheid elements as well as membranes such as pits that transport water and ions [15]. The hierarchical porous structures in wood, ranging from the macroscale to the nanoscale, make it a potential functional material for liquid absorption and fluid filtration, and therefore also for PCMs encapsulation [28,29]. As such, the removal of non-cellulosic components from the cell walls have been considered in the development of anisotropic 3D porous scaffolds. These efforts expanded the porosity and removed obstructions related to mass and energy transport in wood, *via* highly oriented cellulose micro- and nanofibrils [30-32]. Compared with natural wood, these scaffolds exhibit lower density, larger surface area, and higher porosity (up to 95%), paralleling other routes such as those based on cellulose cryogels and aerogels.

Considering its absorption capability in oil/water separation, tropical balsa (*Ochroma pyramidale*) is a good candidate for encapsulation of PCM. This is because the high fiber tracheids content (80% to 90% [33]), and the reported high oil absorption (as high as 15 g/g [34,35] after functionalization). Wood-based FPCMs have been fabricated by direct delignification of cedar wood slices and subsequent vacuum-assisted impregnation with capric-palmitic acid [36]. The obtained FPCMs showed relatively high encapsulation capability (~61 %). The near complete removal of hemicellulose and lignin by using NaOH/Na₂SO₃ treatment facilitated high porosity and a reasonable PCM uptake. However, this treatment degraded the cell wall structure and reduced the mechanical performance, leading to leakage when subjected to loading. Therefore, the selective removal of hemicelluloses and lignin at the expense of a limited increase of porosity is hypothesized to help retaining the cell structure of natural wood and avoiding its collapse under load.

In this work, we propose light-weighted 3D scaffolds from balsa to sustain high compression loads while encapsulating a PCM for energy management. The initial cellular structure of balsa

was transformed into vertically aligned vascular structures by selectively removing lignin and preserving cellulose and hemicelluloses via a one-step chemical treatment [34]. Thus, we hypothesize that selective removal of lignin improves the scaffold permeability through extensive pore structuring at the macro- and mesoscales. We further hypothesize that residual hemicelluloses are critical in preserving a network with aligned cellulose fibrils, yielding a stable and strong 3D scaffold that is fully suitable to hold and protect PCMs even under external forces. The proposed anisotropic vascular structure is tested for its thermal storage performance while keeping in mind attributes such as cost-effectiveness, sustainability and facile processing, all of which are critical to fulfill the future demands for thermal energy storage and conversion.

2. Experimental

2.1 Materials

Balsa wood (*Ochroma pyramidale*), $87.7 \pm 3.2 \text{ mg/cm}^3$ density, was acquired from Modulor, Berlin, Germany and used in the fabrication of encapsulating vessel scaffolds. Before use, the wood was first oven-dried at 90°C for 24 h and then sawed into small cubic segments ($\sim 1 \text{ cm}^3$). Sodium chlorite (NaClO_2 , $\geq 90\%$), sodium hydroxide (NaOH), and polyethylene glycol (PEG, 1500 g/mol) were supplied by Sigma-Aldrich. Other chemicals including acetic acid and anhydrous ethanol ($\geq 99.5\%$) were provided by HyClone (USA). Deionized (DI) water was used in all experiments.

2.2 Preparation of balsa-based, vertically aligned microfibers

3D scaffolds with vertically aligned structures were obtained by selective delignification and optional hemicellulose removal from the cell wall of balsa wood. Stable structures were formed after lyophilization. Typically, oven-dried balsa cubic blocks were first immersed in DI water overnight for complete infiltration. The wet wood blocks were transferred into aqueous 1 wt% NaClO_2 solution and pH 4.6 using acetic acid and kept at 100°C for the removal of lignin. The

delignified wood samples were boiled in DI water and washed several times until the greenish-yellow rinsing water turned colorless. Finally, the samples were frozen (-18 °C) and freeze-dried. Optionally, such wood derived vessel scaffolds were further treated with 10 wt% NaOH aqueous solution to remove hemicelluloses and then rinsed several times. After freeze-drying the lignin- and hemicellulose-free samples formed a porous solid comprising cellulose nanofibrils that was used for comparison.

2.3 Preparation of balsa-based composite PCMs (FPCMs).

Composite PCMs were prepared by vacuum impregnation. Firstly, solid flakes of PEG 1500 were melted on a hot plate. Then, the as-prepared balsa-based scaffolds were immersed in the melted PEG and transferred into a vacuum oven at 80 °C (-0.1 MPa). During this process, the air in the micro/mesoporous structures was removed to allow PEG infiltration to the whole sample. After 1 h, the vacuum was turned off, which promoted PEG penetration. The vacuum and infiltration process were cycled four times to ensure the incorporation of PEG. After the vacuum impregnation, the wood scaffolds were removed from (liquid) PEG and the degree of leakage was determined to calculate the encapsulation capacity of the FPCM. The impregnated wood scaffolds were placed on filter paper in an oven of 80 °C, to remove free PEG from the sample surfaces. During this period, the contact surface was replaced every 10 min to ensure the removal of free PEG. In addition, the filter paper was continuously replaced until no PEG leaking was observed. The weight of the as-prepared wood-based FPCM was recorded every 60 min. Finally, the encapsulation capacity of the FPCM was obtained by calculating the mass of residual PEG after heating. For comparison, composite PCMs based on untreated wood and cellulose nanofiber scaffolds were used as encapsulating material, following the methods above.

2.4 Characterization

The chemical composition of all samples was determined by Fourier transform infrared spectroscopy (FTIR, ATR mode) in the 400-4000 cm^{-1} range, 4 cm^{-1} resolution. The morphology of the samples were observed by using field emission scanning electron microscopy (SEM, Zeiss Sigma VP) operating at an accelerating voltage of 10 kV. The main components in untreated wood were tested in accordance to the NREL/TP-510-42618 analytical method, issued by the National Renewable Energy Laboratory (NREL). Briefly, the acid insoluble lignin content was confirmed by sulfuric acid (72 wt%) hydrolysis. The hemicellulose and α -cellulose content were calculated based on sugar analyses using high-performance anion exchange chromatography (Dionex 3000). The mesoporosity was determined with a Micromeritics Tristar II 3020 instrument utilizing N_2 adsorption and desorption. The specific surface area (SSA) was calculated according to Brunauer-Emmett-Telle (BET) analysis. The thermal properties of pure PEG and balsa-based FPCMs, before and after 200 heating/cooling cycles, were examined with a differential scanning calorimeter (DSC) operating from 5 to 65 $^{\circ}\text{C}$ (5 $^{\circ}\text{C}/\text{min}$ rate) under nitrogen. The compression strength of the scaffold in the longitudinal (vessel or axial direction) was conducted using a universal mechanical testing unit (Instron, 4204) using a 25-N load cell.

2.5 Thermal storage and recovery measurements

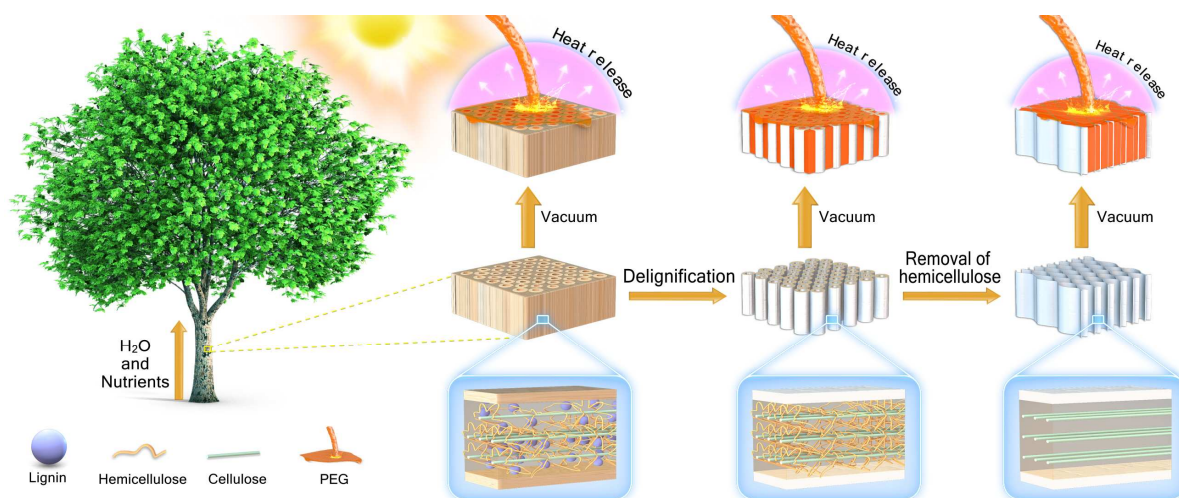
The thermal storage and release of balsa-based FPCMs was investigated by using a PT100 thermometer coupled with a temperature detection apparatus in a designed setup. Briefly, 27 blocks of balsa-based FPCMs were stacked together to form a bulk cube (a side length around 30 mm), followed by sealing with an aluminum foil. A calibrated PT100 thermometer was then inserted into the core of the as-stacked bulk composite PCMs. Then, the cube was placed into a plastic tube, followed by heating to 60 $^{\circ}\text{C}$ using a water bath until the temperature remained constant. Next, the heated tube was rapidly transferred into an ice-bath to trigger the release of latent heat. The temperature was automatically recorded every 2 s during repeated heating/cooling cycles. For comparison, the thermal storage and recovery properties of the reference samples

(untreated wood scaffold and that comprising cellulose nanofibrils) were measured following the same procedures.

3. Results and Discussion

3.1 Balsa-based scaffolds

The fabrication of balsa-based 3D scaffolds for thermal energy management (form-stable composite phase change materials, FPCMs) is illustrated in Scheme 1. So far, untreated wood has been shown to have limited PCM encapsulating ability because of its discontinuous pore structure [37]. On the other hand, anisotropic wood-based aerogels, obtained after $\text{Na}_2\text{SO}_3/\text{H}_2\text{O}_2$ treatment, which completely remove lignin and hemicellulose, have expanded the scaffold porosity to values as high as 95% [32]. Compared to unmodified wood, a 15% increase in encapsulation was measured for 1-tetradecanol for the purpose of thermal energy storage [10]. Despite the promising results and the compression strength, these FPCMs are still susceptible to leakage under external forces. This motivated our choice of sodium chlorite (NaClO_2) to selectively remove lignin while preserving the hemicelluloses in wood. Thus, the central hypothesis in this investigation is that a stable, cross-linked structure is maintained *via* the network that is preserved with the hemicelluloses and aligned cellulose microfibrils, both of which enhance the dimensional stability of 3D scaffolds. Subsequent removal of hemicelluloses via alkali treatment was applied to compare the different FPCMs for their encapsulation and structural stability as well as thermal performance.



Scheme 1. Schematic illustration of the fabrication of wood-based 3D scaffold for solar thermal energy storage. Wood blocks (middle row) include, from left to right, natural wood (W); delignified wood (W-L), and delignified wood followed by removal of hemicelluloses (W-L,H). The bottom row illustrates the possible structure and composition of the respective materials. Form-stable phase-changing composite materials (FPCMs), obtained after PEG loading by vacuum-assisted impregnation, are shown in the upper row. From left to right: (W+P), (W-L+P) and (W-L,H+P).

Balsa wood (*Ochroma pyramidale*) ($87.7 \pm 3.2 \text{ mg/cm}^3$) was first boiled in 1% NaClO_2 solution (pH 4.6) to remove lignin. After 18 h, the lignin content was reduced from $23.3 \pm 1.2\%$ to $3.8 \pm 1.4\%$ (Figure S1). This delignified wood is thereafter referred to as W-L. Subsequent reaction with 10 wt% NaOH solution for up to 6 h reduced the hemicellulose content of W-L, from $24.7 \pm 1.1\%$ to $5.6 \pm 1.4\%$ (Figure S2). The delignified wood, with such reduced amount of hemicelluloses is thereafter referred to as W-L,H. The removal of the wood components from balsa wood was confirmed by FITR analysis, Figure S3a. For the untreated balsa wood, two strong absorption peaks occurred at $\sim 1736 \text{ cm}^{-1}$ and 1235 cm^{-1} , assigned to the stretching vibrations of C=O (carbonyl groups) and -CO-OR (ester groups), respectively [38], both are fingerprints for hemicelluloses (amorphous polysaccharides). Also, weak peaks at 1590 cm^{-1} , 1505 cm^{-1} , and 1462 cm^{-1} correspond to aromatic skeletal vibrations assigned to lignin [39]. After treatment with NaClO_2 solution, the characteristic peaks of lignin disappeared while those

associated with hemicelluloses were preserved, indicating selective removal of lignin. For W-L,H, the peaks characteristic of hemicelluloses were absent, indicating the extensive removal of hemicelluloses after NaOH solution treatment. The changes in chemical composition for the three samples are shown in Figure S3b.

Figure 1 includes a schematic illustration of the macroscale morphology and axial cross-section of untreated balsa wood, and scaffolds based on delignified wood (W-L), and delignified wood after removal of hemicelluloses (W-L,H), as well as the respective FPCMs, after PEG loading ((W+P), (W-L+P), (W-L,H+P)). The balsa wood presents a distinct pale yellow color (Figure 1a1), which is the result of two lignin chromophores, conifer aldehyde and aromatic ketones [40]. At the micron scale, the tracheids show a double cell wall thickness of 1.5~2 μm , forming a honeycomb-like, hollow structure with vascular lumens with average diameter of ~20 μm (Figure 1a2, 1a3). The thin wall structure (membrane) between neighboring tracheids and homogeneously disturbed pits are apparent in the longitudinal sections (Figure S4a2, 4a3). After delignification with NaClO_2 , the chromophoric groups disappear, which make the resultant scaffold to turn white in color (Figure 1b1). The thickness of the cell wall layer becomes thinner (Figure 1b3). Separated vertically-aligned vascular structures are observed in the cross section (Figure 1b2). The changes in the hierarchical cell wall structure of the balsa wood are the result of the removal of the lignin-rich primary wall and the middle lamella. Thin wall structures with expanded pits explain an increased porosity, $94.8 \pm 1.3 \%$ (Note S1, Figure S4b2, 4b3). Further removal of hemicellulose with NaOH solution affected extensively the morphology of the W-L sample (Figure 1c1). The anisotropically-aligned hexagonal vascular structures observed in the cross and longitudinal sections disappear completely. Deformed cell walls of W-L,H form spring-like lamellar structures with stacking curved layers (Figure 1c2, 1c3 and Figure S4c2), ascribed to individual aligned cellulose microfibrils that remain after removal of lignin and

hemicellulose. It is hypothesized that microfibrils linked with each other by hydrogen bonds are assembled in these lamellar structures (Figure S4c3), which are expected to resist compression.

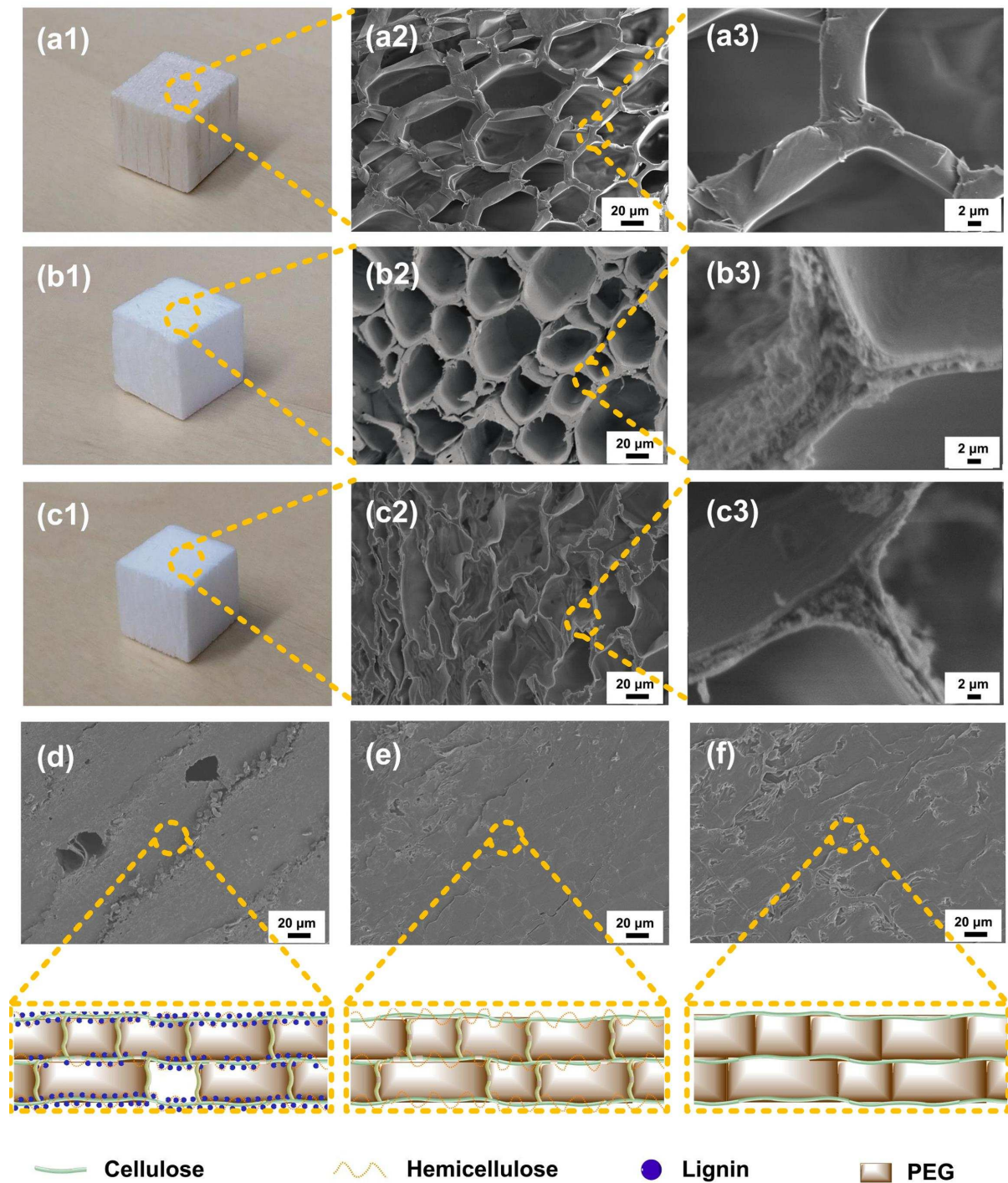


Figure 1. Photographs of untreated balsa wood W (a1), W-L (b1) and W-L,H (c1) and FE-SEM cross-section images at low (a2, b2 and c2) and high (a3, b3 and c3) resolution. Axial section morphology (axial cut for SEM) upon PEG encapsulation (FPCMs) obtained from untreated balsa W+P (d), W-L+P

(e), and W-L,H+P (f). The schematic illustrations in the bottom (from left to right) correspond to speculative structures and chemical makeup of the systems shown above, a1-3, b1-3, c1-3, respectively.

3.2 Form-stable composite phase change materials, FPCMs.

The balsa-based scaffolds (untreated wood W, W-L, and W-L,H) were impregnated with a PCM (PEG), forming the FPCMs ((W+P), (W-L+P) and (W-L,H+P)). As shown in Figure 1d, 1e, 1f, the macro-scale vascular pores of the samples were filled with PEG; no apparent interface separation was observed between the inner, PEG-filled areas and the outer wall of the vessels, suggesting a good affinity between PEG and the walls of the scaffold. However, compared with W-L and W-L,H, which were fully filled with PEG, some holes were observed in the cross section of the untreated wood scaffold. In this latter case, plugged pits and thin wall structures, typical of early age tracheids, created a confined space that prevented PEG transport and led to void areas within the structure [37]. Removal of lignin and hemicellulose expanded the pits and eliminated the thin wall structure between the fibrous tracheids, improving the permeability of the scaffold. A relative high encapsulation degree was observed for the FPCMs. The interactions between PEG and the scaffold in the FPCMs were further investigated by FTIR analyses (Figure S5, S6, and S7). The FTIR spectrum of neat PEG includes a broad absorption peak located at 3430 cm^{-1} , assigned to the stretching vibration of -OH (hydroxyl groups), and a sharp peak at around 2880 cm^{-1} corresponding to the -CH stretching vibration [41]. In the fingerprint zone ranging from 2000 cm^{-1} to 500 cm^{-1} , the asymmetric stretching vibration of -C-O groups were observed at 1110 cm^{-1} . Moreover, the spectral bands at 841 cm^{-1} correspond to the -CH bending vibration. The characteristic FTIR peaks of PEG were all present in the PEG-filled samples based on untreated wood (W+P), delignified wood (W-L+P) and delignified, hemicellulose-free (W-L,H+P) FPCMs. A high intensity of PEG peaks in W-L+P and W-L,H+P indicate a high loading. Most importantly, the absorption peak of -OH in the three FPCMs shifted from 3430 cm^{-1} to 3390 cm^{-1} , suggesting hydrogen bond interactions between the PEG and the substrates [18]. No chemical

interaction exists between PEG and the substrates, which is important in preserving the phase transition performance of the FPCMs.

3.3 Scaffold mesopore distribution and encapsulation capacity

To further investigate the encapsulation of the balsa-based scaffolds, the changes in mesoporosity, before and after PEG impregnation, were followed with Brunauer-Emmet-Teller (BET) measurements. Figure 2a shows the nitrogen gas adsorption-desorption isotherms of untreated wood W, W-L, W-L,H, as well as W-L,H+P. The adsorbed mass for all the samples included a slow rise at the onset, it then grew steadily, and eventually became more extensive at a steep rate. Meanwhile, hysteresis occurred during the desorption process. The profiles indicate type IV isotherms, which are typical of micro- and mesopore with multimodal distribution [34]. The untreated balsa wood exhibited inferior of nitrogen physisorption, with a low specific surface area (SSA), $2.9 \pm 0.4 \text{ m}^2 \text{ g}^{-1}$. After delignification, the SSA increased significantly, $19.2 \pm 1.1 \text{ m}^2 \text{ g}^{-1}$. As expected, the highest nitrogen absorption was observed in the delignified and hemicellulose-free sample (W-L,H) with a SSA value of $24.7 \pm 2.3 \text{ m}^2 \text{ g}^{-1}$. The removal of lignin and hemicellulose also changed the pore volume distribution, Figure 2b. Compared to untreated balsa wood, W-L and W-L,H displayed a distinct nanoscale pore structure, 2-20 nm in diameter. Meanwhile, the more extensive removal of the amorphous matrix from the cell wall in W-L,H correlates with a broad nanopore distribution, with a pore size $< 10 \text{ nm}$, similar to the findings by Guan et al. [35]. Interestingly, the as-prepared FPCMs displayed an large reduction in porosity, ranging from 5 to 90 nm and a very low specific surface are, $\text{SSA} = 0.77 \pm 0.3 \text{ m}^2 \text{ g}^{-1}$, suggesting the filling of W-L,H nanopores with PEG, as suggested by the SEM images (Figure 1f).

A plausible mechanism for the evolution of the nanoscale structure of the scaffolds can be suggested, starting with the untreated wood cell wall, where hemicelluloses form a network with cellulose microfibrils and lignin (Figure 2c1). The dense structure presents a low SSA and limited mesopores. Lignin removal leads to a mesoporous structure in the scaffold (Figure 2c2).

Subsequent chemical treatment with NaOH weakens the interconnected hemicellulose network, resulting in a unidirectional scaffold comprising cellulose microfibrils, with increased mesoporosity (Figure 2c3). Finally, PEG infiltrated the vascular macro and mesoporous structures, initially occupying the original spaces in the amorphous matrix of the cell wall. Combined with cellulose microfibrils, hydrogen bonded PEG produces a dramatic reduction of both in SSA and pore volume (Figure 2c4).

Leakage tests were conducted by holding the PEG-filled FPCMs on a filter paper at 80 °C and measuring the encapsulation capacity as a function of time. As shown in Figure 2d, the residual PEG mass after 8 h holding time was to 53.2 %, 83.5 %, and 87.8 %, for W+P, W-L+P, and W-L,H+P, respectively. The results clearly indicate a better holding or encapsulation capacity for melted PEG after removal of lignin and hemicellulose. Notably, to the best of our knowledge, the encapsulation mass ratios of W-L+P and W-L,H+P samples are clearly higher than those of wood-based and clay-based FPCMs loaded PEG or other PCMs. (Figure 2e).

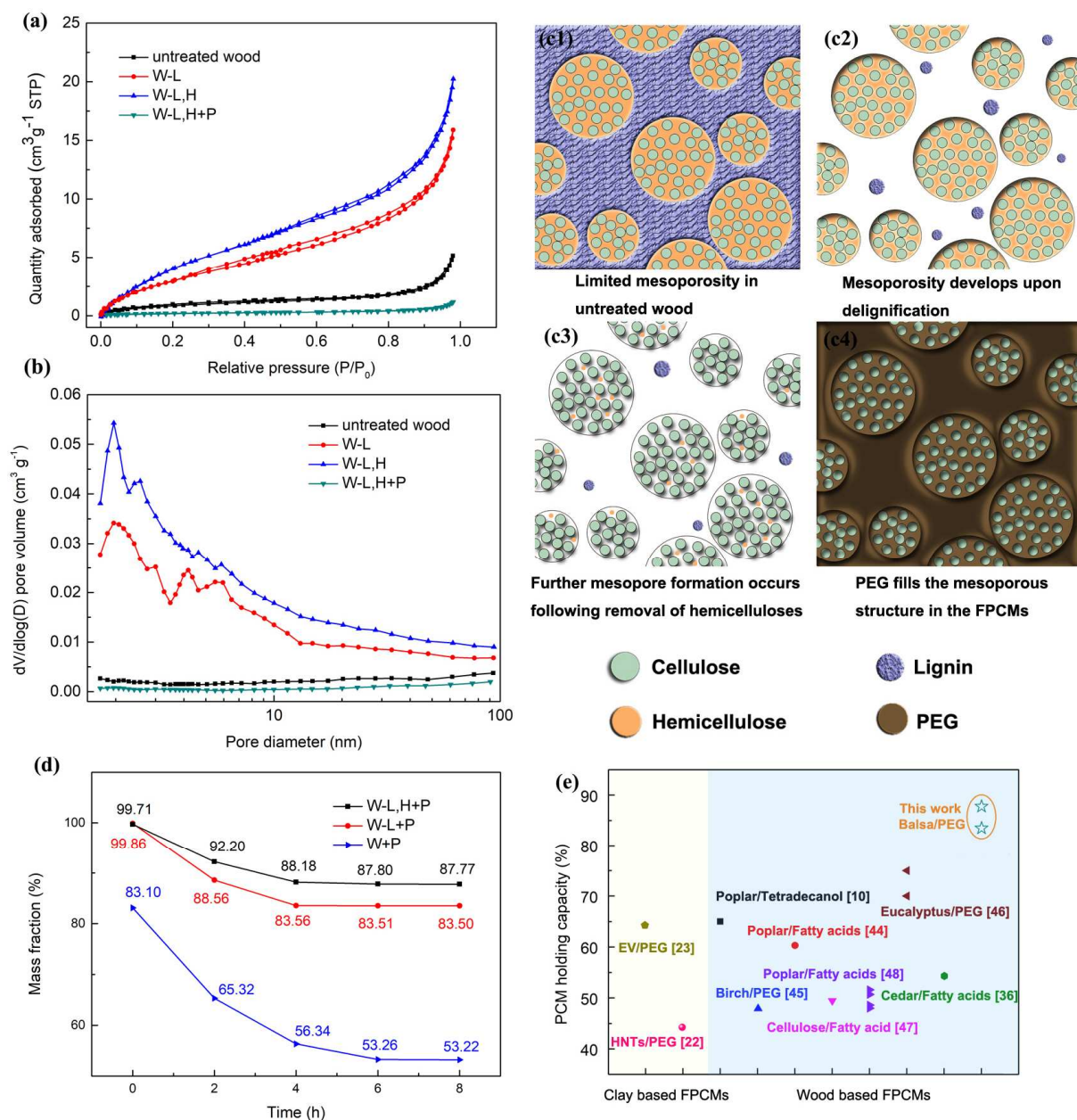


Figure 2. (a) Nitrogen adsorption-desorption isotherms and (b) pore size distribution of untreated wood, W-L, W-L,H, and W-L,H+P. The mechanism of mesopore evolution is shown for (c1) untreated wood W, (c2) W-L, (c3) W-L,H, and (c4) W-L,H+P. (d) Leakage profile (PEG mass fraction as a function of time) of the balsa-based FPCMs. (e) Encapsulation capacity of the wood derived scaffolds prepared in this work compared to other porous materials reported in the literature.

In sum, PEG floods the vascular channels and lumen structures as well as the mesopores within the cell wall of the balsa-based scaffolds *via* strong physical interactions including capillary forces and hydrogen bonding. This support the PEG solid-to-liquid phase transition

while extensively avoiding leakage under heating, reaching plateau values for the liquid PEG mass that is held by the system.

3.4 Thermal properties and phase change behavior of the FPCMs

Practical applications for thermal energy management require a high latent heat storage capacity, suitable phase transition temperature, and durable 3D structures. Differential Scanning Calorimetry (DSC) was used to investigate the thermal properties of the FPCMs as well as their phase transition behavior. Figure 3a shows the DSC curves of pure PEG and the FPCMs (untreated wood W, W-L+P, and W-L,H+P) during endothermic and exothermic cycles. The main results from the DSC curves are shown in Table 1, including the melting temperature (T_m), melting enthalpy (ΔH_m), crystallization temperature (T_c), and crystallization enthalpy (ΔH_c). In addition, the effective enthalpy content (F) of the FPCMs is included, which was calculated as follows [49]:

$$F = \frac{\Delta H_{FPCM}}{\Delta H_{Pure\ PEG}} \times 100\%$$

ΔH_{FPCM} and $\Delta H_{Pure\ PEG}$ represents the measured crystallization enthalpy for the FPCM and that of neat PEG ($158.4\text{ J}\cdot\text{g}^{-1}$), respectively. As shown in Figure 3a, the DSC curves of the FPCMs are similar to those of pure PEG, showing an endothermic and an exothermic peak corresponding to the solid-liquid and liquid-solid phase transitions. This indicates that PEG was encapsulated in the scaffolds while retaining its inherent phase change properties, given that no chemical interactions occurred. A high thermal energy storage capacity with phase transition enthalpy close to that of the neat PCM is desirable for a wide utilization in thermal storage. During the melting and solidification process, the phase transition enthalpies of pure PEG are $168.2\text{ J}\cdot\text{g}^{-1}$ and $158.4\text{ J}\cdot\text{g}^{-1}$, respectively. As for the PEG-filled, untreated balsa wood, the respective enthalpy values were $95.0\text{ J}\cdot\text{g}^{-1}$ and $83.7\text{ J}\cdot\text{g}^{-1}$. Compared with the untreated wood, the phase transition enthalpy values for the FPCMs based on treated wood increased as the amorphous components were removed.

W-L+P had a melting and solidification enthalpy of $134.3 \text{ J}\cdot\text{g}^{-1}$ and $125.3 \text{ J}\cdot\text{g}^{-1}$, respectively. Despite the higher PEG encapsulation capacity for W-L,H+P, the enthalpy values remained approximately the same $135.0 \text{ J}\cdot\text{g}^{-1}$ and $126.1 \text{ J}\cdot\text{g}^{-1}$. This is desirable since the support should affect minimally the crystallinity of the contained PCM [18] and maintain the enthalpies values as close as possible to that of the neat PCM. Table 1 indicates that the measured effective enthalpy content (F) of untreated wood FPCM is 52.8%. To put the data in perspective, we use an ideal enthalpy content (I) based on the limiting PEG fraction that is retained after 8 h in the melted state ($I=53.2\%$ for untreated wood) for a F/I (the ratio of the measured effective enthalpy content (F) and ideal phase transition enthalpy (I)) equivalent to 0.99. For W-L+P and W-L,H+P the calculated F/I amounts to 0.95 and 0.91, respectively, indicating the tradeoff between mass loading and PEG encapsulation and the retention of the crystallization enthalpy.

As we mentioned above, the confined PEG reduces the enthalpies and crystallinity values of composite PCMs, resulting in a lower effective enthalpy content (F) than the ideal value (I). To better elucidate the influence of the main components in the wood cell wall on PEG crystallinity, an additional experiment was conducted (Note S2 and Figure S10) where a series of incompletely filled FPCMs were prepared (with reduced PEG content in the lumens). Figure 3c summarizes the F/I value of the different FPCMs as a function of PEG loading. A downward trend is noted for the FPCMs with PEG loading, indicating that the balsa-based supports affected the crystallinity of the encapsulated PEG. Expectedly, compared to the untreated wood, a decreasing trend for F/I was shown for chemically treated wood FPCMs; the W-L,H+P system showed the lowest F/I value, with the PEG mass fraction of 20 %. The results are rationalized by the interactions of PEG with hydroxyl groups, as has been shown for silica, which immobilizes PEG molecules by hydrogen bonds, resulting in a change in the crystallization or phase transition of the confined PEG compared to that of neat PEG [42]. The available hydroxyl groups in cellulose and wood-derived scaffolds play an important role in the crystallization of

encapsulated PEG. Among the wood components, hydrophobic lignin presents an inferior affinity with hydrophilic PEG. For untreated wood, lignin fills the aligned cellulose microfibrils, which reduce the effective adsorption sites (-OH) on the cellulosic surfaces to hydrogen bond with PEG (Figure 3d). Therefore, untreated wood has the lowest effect in the crystallization behavior of PEG, resulting in no significant reduction of phase transition enthalpy. The removal of lignin facilitated hydrogen bonding with cellulose and hemicellulose, hindering the crystallization of PEG in W-L+P (Figure S8a). This effect was further promoted by the removal of hemicellulose in W-L,H+P (Figure S8b). Thus, while the PEG encapsulation capacity and its retention in the liquid state was increased by the removal of lignin and hemicelluloses, PEG crystallization was simultaneously affected, leading to differences in phase transition enthalpy.

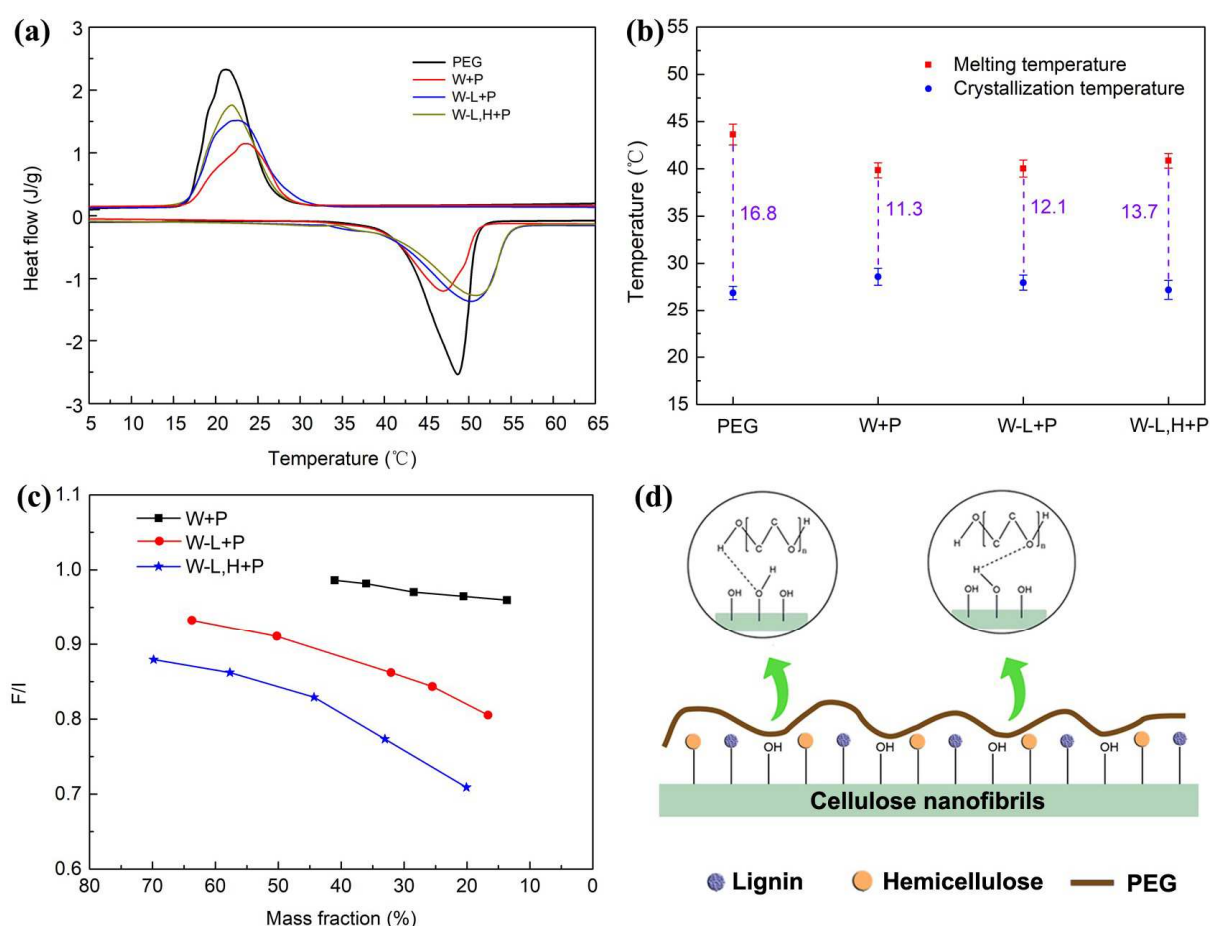


Figure 3. Thermal performance of balsa-based FPCMs. DSC curves (a) and the degree of supercooling (b) of neat PEG, W+P, W-L+P, and W-L,H+P. The ratio of experimental phase change enthalpy to the

theoretical phase change enthalpy for different PEG mass loading in the FPCMs (c). Schematic illustration of the interactions between PEG and the FPCM scaffolds in W+P (d).

Considering the phase change temperature of FPCMs, which should respond to external environmental changes, the difference between melting and crystallization temperature (the supercooling degree), is an important factor to consider in any practical application. Neat PEG has a high degree of supercooling (16.8 °C), which prevents the release of the as-stored thermal energy when the crystallization temperature is much lower than the melting temperature, Figure 3b. Our PEG's degree of supercooling is within reported values, between 10 and 20 °C [17]. After PEG encapsulating in balsa-based scaffolds, the extent of supercooling is reduced to 11.3, 12.1 and 13.7 °C for untreated wood W+P, W-L+P, and W-L,H+P, respectively. While the addition of a nucleating agent can be used to reduce the supercooling degree [43], we note that the results indicate that untreated wood serves as good candidate for PEG nucleation, decreasing the supercooling by 5.5 °C. For the rests of FPCMs, the supercooling degree gradually increases with the reduction of the relative content of amorphous matrix within wood cell walls. Thus, selective removal of lignin and hemicelluloses exposes adsorption sites for PEG, inhibiting nucleating and further crystallization. All values for the degree of supercooling reported here for the FPCMs are lower than that of pure PEG. Moreover, the phase transition temperature of W-L+P, and W-L,H+P is optimal for uses at the outdoor temperatures prevalent in the summer season. Therefore, the proposed FPCMs have a great potential for thermal energy conversion and management, especially for passive solar heating applications.

In addition to optimal thermal properties, a stable FPCM structure is critical for any deployment. FPCMs need to demonstrate excellent durability with no PCM leakage when the ambient temperature is higher than the PCM's melting point. Wood possesses superior mechanical properties because of its unique hierarchical structure within the cell walls. The removal of wood's amorphous matrix increases permeability; inevitably, this is at the expense of

cell walls with lower mechanical strength. To test these effects, we measured the mechanical compressibility of balsa-based scaffolds, before and after treatment.

Table 1. The DSC data for neat PEG and balsa-based FPCMs.

Samples	Melting process		Solidification process		$F/\%$	$I/\%$	F/I
	$T_m/$	$\Delta H_m/\text{J}\cdot\text{g}^{-1}$	$T_c/$	$\Delta H_c/\text{J}\cdot\text{g}^{-1}$			
PEG	43.6	168.2	26.9	158.4	100	100	1.00
W+P	39.8	95.0	28.6	83.7	52.8	53.2	0.99
W-L+P	40.0	134.3	27.7	125.3	79.1	83.5	0.95
W-L,H+P	40.9	135.0	27.2	126.1	79.6	87.8	0.91

Note: Ideal phase transition enthalpy (I) of the prepared FPCMs is calculated using PEG mass loading per unit mass (%).

Under the applied load, it was not possible to compress the native balsa along the longitudinal direction (Figure S9a1). After removal of lignin, the wood blocks (W-L) was compressed only under a very large loading. It recovered, to a large extent, its initial dimensions upon unloading (Figure S9b1). Further removal of hemicellulose in the W-L,H block facilitated compression and recovery of the original shape (Figure S9c1). This is also shown in the stress-strain profiles included in Figures S9a2, 9b2, 9c2. Recent studies have focused on FPCMs by complete removal of lignin and hemicellulose from wood [10, 36]. However, considering the observed compressibility, leakage is expected to occur under external loading. To assess possible PEG leaking in our FPCMs, W-L+P and W-L,H+P were heated to 100 °C and the samples were observed under load. Figure 4a shows the solid-to-liquid transition for neat PEG. A 200-g load with the pressure of 2 kPa was placed on top of the FPCMs during the heating process to demonstrate their mechanical strength and holding capacity (for the melted PEG). As shown in Figure 4b, after cooling and removing the load, the W-L+P retained its original shape, with no signs of PEG leaking. Unfortunately, some limited PEG leaking was observed in the case of W-L,H+P (Figure 4c).

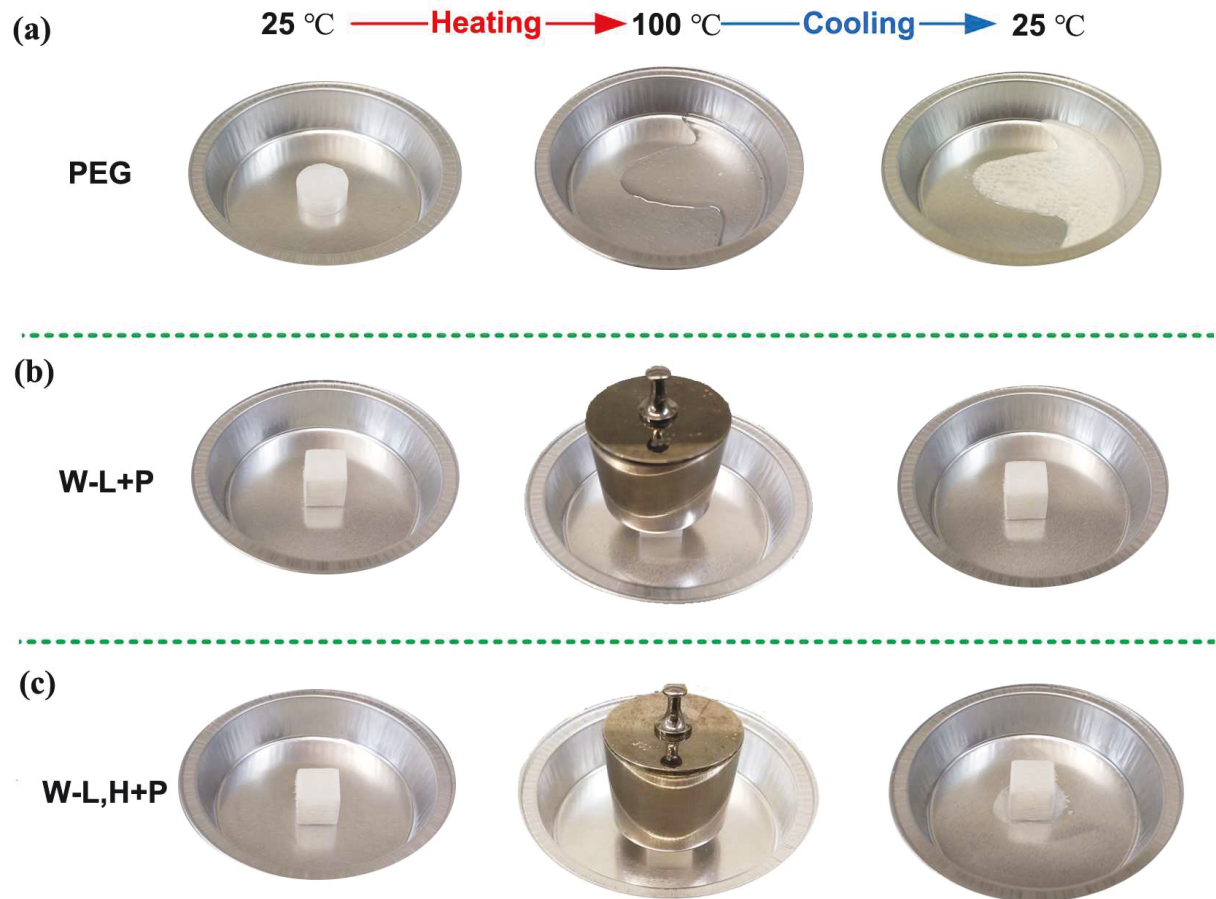


Figure 4. Leakage tests for pure PEG (a) and for wood derived composite PCMs under external force and longitudinal vascular direction W-L+P (b) and W-L,H+P (c).

Table 2. Performance of FPCMs in the current work compared with those based on other wood composite containing given PCMs.

FPCM	Melting T (°C)	Crystallization T (°C)	Latent heat (J/g)	Encapsulation ratio (%)	Ref.
Douglas fir/PEG	36.1	26.7	73.6	34.3	[37]
Poplar/1-tetradecanol	35.2	34.3	118.5	65	[10]
Poplar/Lauric-myristic acid	33.1	32.9	98.2	60.3	[44]
Birch/PEG	38.3	28.6	76.3	49	[45]
Eucalyptus/PEG 1000	47.7	22.2	108.6	75	[46]
Cedar/Capric-palmitic acid	23.4	14.5	94.4	61.2	[36]
Delignified balsa/PEG	40.0	27.7	134.3	83.5	This work

To conclude, FPCMs based on delignified balsa wood have a high latent heat, with suitable PEG encapsulation and holding abilities (Table 2). In addition, our FPCMs have a small supercooling degree, suitable phase change temperature, and superior mechanical resistance. A one-step selective delignification (NaClO_2) is more efficient than the process used so far based on non-selective, two-step processing ($\text{Na}_2\text{SO}_3/\text{NaOH}$ and H_2O_2). Thus, hemicellulose-containing balsa scaffolds, with vertically-aligned vascular structures, can fit the criteria for a porous carrier for PEG encapsulation and for uses in thermal energy storage.

3.5 FPCM's cyclical thermal performance

An ideal FPCM should maintain its original thermal properties as well as structure (chemical, physical) after cycles of heat storage and release. We tested our FPCMs after 200 heating and cooling cycles (DSC profiles of W-L+P, Figure 5a). The initial melting and crystallization peaks and enthalpies of melting/crystallization were largely preserved after 200 cycles (Figure 5b and 5c, respectively). After thermal cycling, the latent heat of melting and cooling was only reduced by 0.6 % and 0.5%, respectively. Consistently, both the melting and crystallization temperatures exhibited slight changes compared with the initial state, increasing only by 1.5 °C and 1.7 °C, respectively. These fluctuations are reasonable for application in thermal devices. FTIR analyses were carried out to follow changes in chemical fingerprints of the FPCMs after 200 thermal cycling. They revealed no effect on the chemical integrity of the delignified balsa wood. Thus, the FPCMs possessed superior thermal and chemical tolerance, held the original latent heat as well as the melting/solidifying point after 200 heating-cooling cycles. The results indicate that these FPCMs are stable and reliable for practical reversible thermal energy storage and retrieval applications.

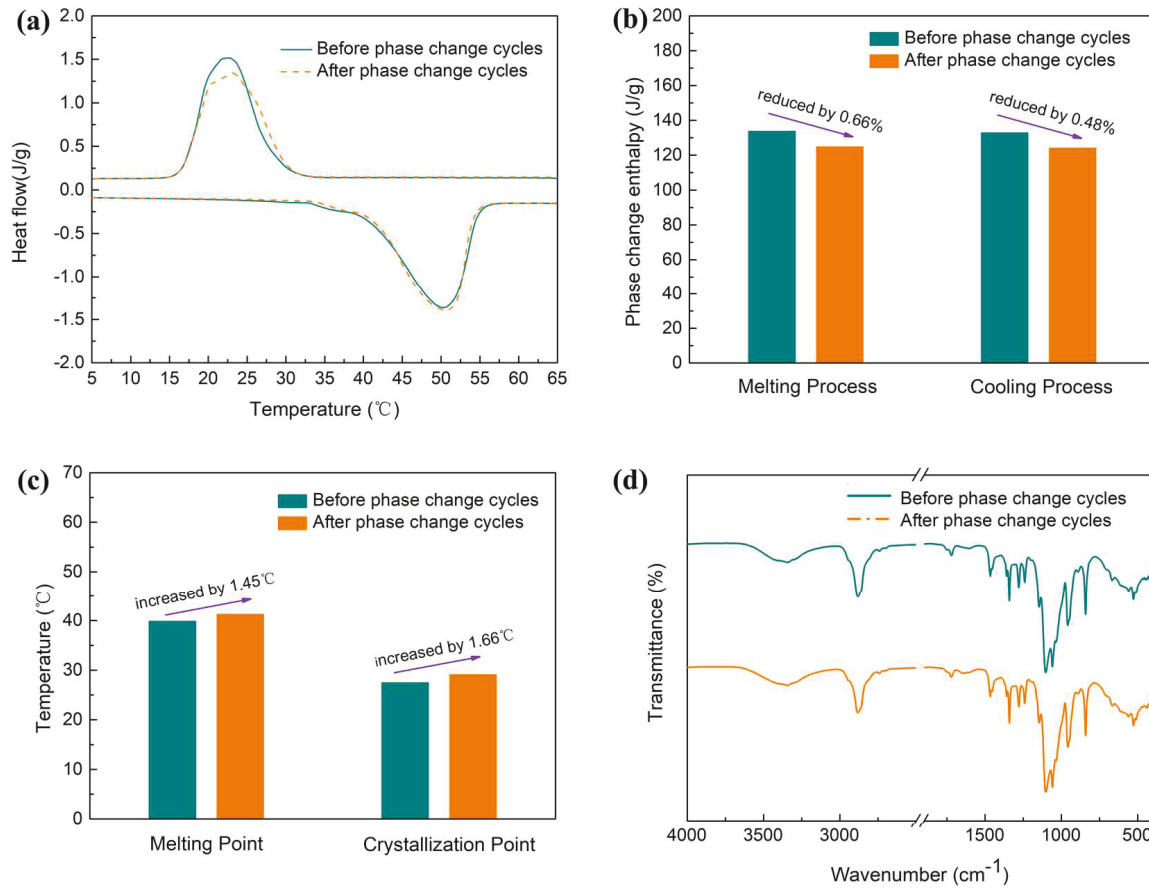


Figure 5. Thermal reliability test results of W-L+P before and after 200 heating-cooling cycles: (a) DSC curves, (b) a summary of phase change enthalpies, (c) melting-and crystallization temperatures, and (d) FTIR spectra.

3.6 Thermoregulatory capacity of balsa-based FPCMs

To evaluate the potential of delignified balsa wood for temperature regulation and thermal storage and retrieval, we compared the temperature changes of the delignified wood scaffold (W-L) and respective FPCM (W-L+P) during heating and cooling cycles. The corresponding thermal storage and retrieval profiles show the core temperature of the samples, Figure 6. Heating W-L from 10 to 48.7 °C took 513 s, without showing any thermoregulatory capacity. In contrast, the heating rate for W-L+P was prolonged when the temperature reached a value close to the melting point of PEG, thus resulting in an extended heating time, 1200 s, until reaching 48.7 °C. Correspondingly, the cooling process from 40 to 0 °C was fast (322 s) for W-L (Figure 6b). For W-L+P, the crystallization of PEG generated an increased cooling time, up to 697 s and

slowed down around 28 °C. The prolonged rate of heating and cooling of W-L+P (twice compared to W-L), indicate an FPCM with superior thermoregulatory capacity. It can be used to reliably harvest, transport, and utilize thermal energy for applications at ambient temperatures, especially for interior temperature regulation.

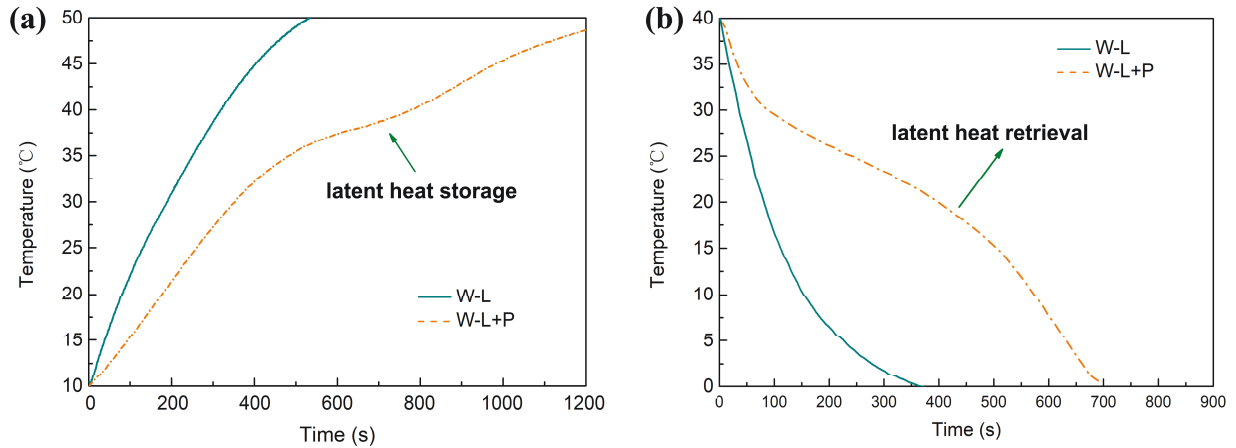


Figure 6. Thermal storage (a) and retrieval (b) profiles for W-L and W-L+P (FPCMs with encapsulated PEG used as PCM).

To conclude, higher plants comprise sophisticated vascular and porous structures that are optimized for absorption and conduction. They are effective in converting solar energy into bioenergy. As a component of wood cell walls, cellulose microfibrils form a stiff skeleton with intertwined lignin and hemicelluloses. Inspired by the unique structural and functional characteristics of the plant cell wall, 3D scaffolds are found to be effective in encapsulating a PCM via capillary forces and hydrogen bonding. The performance of the derived FPCMs, however, depends on a subtle balance of effects brought by the relative concentration of lignin and hemicelluloses, as shown in this investigation.

4. Conclusions

In summary, novel three-dimensional porous scaffolds were successfully developed following green and sustainable wood nanotechnology by selectively eliminating the amorphous

components from natural balsa wood, followed by drying. The as-prepared scaffolds possessed a special hollow structure with numerous vertically aligned vessel structures. The removal of lignin from the structures expands the pore structure, both in macroscale and mesoscale, improving the permeability of the system. Maintaining hemicellulose within the structure served as a cross-linking agent and granted compressive resistance to the hollow structures. Subsequently, PEG was vacuum-impregnated into the hollow vascular lumen structures as well as to the mesopores created by the uniaxial aligned cellulose nanofibrils within the cell wall. The high porosity, together with low density and superior mechanical properties, endowed the composite PCMs with high encapsulation capability, up to 83.50 % and excellent dimensional stability and resistance to external loads. The loading of PEG in the wood scaffold promoted the phase transition properties of the composite PCM. Consequently, the final FPCMs exhibited a highly desirable phase transition temperatures, with melting and crystallization points of 40.0 and 27.7 , respectively. They fit well the demands of outdoor environments during summer. Latent heats of 134.3 J/g for melting enthalpy and 125.3 J/g for crystallization enthalpy were obtained, which are noticeably higher than the ones previously reported for wood-based FPCMs. In addition, FPCM based on delignified balsa wood showed robust thermal and chemical reliability over 200 continuous heating/cooling cycles, showing no deterioration of latent heat nor phase transition temperature fluctuation. Moreover, the introduced FPCM exhibited a longer time for thermal energy storage and release during the heating and cooling processes, increased by two folds compared to the pristine delignified wood scaffold without encapsulated PEG. Therefore, in view of the high latent heat, optimal phase transition temperature, high durability, superior shape stability, robust thermal reliability and suitable thermoregulatory capacity, we suggest that the obtained FPCM offer a competitive alternative, especially considering the low cost, high efficiency, renewability, and easy operation. Altogether, we demonstrate a great potential for the proposed FPCM for thermal energy storage and conversion.

Supplementary Materials:

Porosity of balsa wood; lignin and hemicellulose content in balsa wood during the removal process over time; FTIR analysis of untreated wood, W-L, W-L,H, W-L+P, W-L,H+P, and pure PEG; digital photograph of untreated wood and its longitudinal FE-SEM cross-section images; schematic illustration of the interactions between PEG and the FPCM scaffolds; mechanical properties test of different wood scaffolds; data of the results of BET test; FPCMs with partially loaded with PCM.

Acknowledgements

This work was supported by the European Research Council (ERC) under the European Union's Horizon 2020 research and innovation program (ERC Advanced Grant Agreement No. 788489, "BioElCell"). In addition, the Canada Excellence Research Chair initiative, the Academy of Finland Centre of Excellence in Molecular Engineering of Biosynthetic Hybrid Materials, and the China Scholarship Council (CSC) are gratefully acknowledged for funding support. We are also thankful to Dr. Haiming Li for his help in balsa wood chemical analysis.

References

- [1] Huang, J.L., Zhao, B.T., Liu, T., Mou, J.R., Jiang, Z.J., Liu, J., Li, H.X., Liu, M.L. Wood-Derived Materials for Advanced Electrochemical Energy Storage Devices. *Adv Funct Mater* 2019;29:1902255.
- [2] Zhu, H.L., Luo, W., Ciesielski, P.N., Fang, Z.Q., Zhu, J.Y., Henriksson, G., Himmel, M.E., Hu, L.B. Wood-Derived Materials for Green Electronics, Biological Devices, and Energy Applications. *Chem Rev* 2016;116:9305-9374.
- [3] Wang, H., Jasim, A., Chen, X.D. Energy harvesting technologies in roadway and bridge for different applications - A comprehensive review. *Appl Energy* 2018;212:1083-1094.

- [4] Huang, X.B., Chen, X., Li, A., Atinafu, D., Gao, H.Y., Dong, W.J., Wang, G. Shape-stabilized phase change materials based on porous supports for thermal energy storage applications. *Chem Eng J* 2019;356:641-661.
- [5] Zhu, N., Li, S.S., Hu, P.F., Wei, S., Deng, R.J., Lei, F. A review on applications of shape-stabilized phase change materials embedded in building enclosure in recent ten years. *Sust Cities Soc* 2018;43:251-264.
- [6] Yang, J., Tang, L.S., Bao, R.Y., Bai, L., Liu, Z.Y., Xie, B.H., Yang, M.B., Yang, W. Hybrid network structure of boron nitride and graphene oxide in shape-stabilized composite phase change materials with enhanced thermal conductivity and light-to-electric energy conversion capability. *Sol Energy Mater Sol Cells* 2018;174:56-64.
- [7] Wang, Y.M., Tang, B.T., Zhang, S.F. Single-Walled Carbon Nanotube/Phase Change Material Composites: Sunlight-Driven, Reversible, Form-Stable Phase Transitions for Solar Thermal Energy Storage. *Adv Funct Mater* 2013;23:4354-4360.
- [8] Miro, L., Gasia, J., Cabeza, L.F. Thermal energy storage (TES) for industrial waste heat (IWH) recovery: A review. *Appl Energy* 2016;179:284-301.
- [9] He, Y., Li, W., Han, N., Wang, J., Zhang, X. Facile flexible reversible thermochromic membranes based on micro/nanoencapsulated phase change materials for wearable temperature sensor. *Appl Energy* 2019;247:615-629.
- [10] Yang, H.Y., Wang, Y.Z., Yu, Q.Q., Cao, G.L., Yang, R., Ke, J.N., Di, X., Liu, F., Zhang, W.B., Wang, C.Y. Composite phase change materials with good reversible thermochromic ability in delignified wood substrate for thermal energy storage. *Appl Energy* 2018;212:455-464.
- [11] Guo, X., Liu, C., Li, N., Zhang, S., Wang, Z. Electrothermal Conversion Phase Change Composites: The Case of Polyethylene Glycol Infiltrated Graphene Oxide/Carbon Nanotube Networks. *Ind. Eng. Chem. Res.* 2018;57:15697-15702.
- [12] Du, J., Sheng, L., Chen, Q., Xu, Y., Li, W., Wang, X., Li, M., Zhang, S.X. A. Simple and general platform for highly adjustable thermochromic fluorescent materials and multi-feasible applications. *Mater Horizons* 2019;6:1654-1662.
- [13] Lyu, J., Liu, Z., Wu, X., Li, G., Fang, D., Zhang, X. Nanofibrous Kevlar Aerogel Films and Their Phase-Change Composites for Highly Efficient Infrared Stealth. *ACS Nano* 2019;13:2236-2245.

- [14] Lu, Y., Xiao, X.D., Fu, J., Huan, C.M., Qi, S., Zhan, Y.J., Zhu, Y.Q., Xu, G. Novel smart textile with phase change materials encapsulated core-sheath structure fabricated by coaxial electrospinning. *Chem Eng J* 2019;355:532-539.
- [15] Pielichowska, K., Pielichowski, K. Phase change materials for thermal energy storage. *Prog Mater Sci* 2014;65:67-123.
- [16] Sarier, N., Onder, E. Organic phase change materials and their textile applications: An overview. *Thermochim Acta* 2012;540:7-60.
- [17] Kou, Y., Wang, S.Y., Luo, J.P., Sun, K.Y., Zhang, J., Tan, Z.C., Shi, Q. Thermal analysis and heat capacity study of polyethylene glycol (PEG) phase change materials for thermal energy storage applications. *J Chem Thermodyn.* 2019;128:259-274.
- [18] Wang, J.J., Yang, M., Lu, Y.F., Jin, Z.K., Tan, L., Gao, H.Y., Fan, S., Dong, W.J., Wang, G. Surface functionalization engineering driven crystallization behavior of polyethylene glycol confined in mesoporous silica for shape-stabilized phase change materials. *Nano Energy* 2016;19:78-87.
- [19] Mellouli, S., Askri, F., Abhilash, E., Ben Nasrallah, S. Impact of using a heat transfer fluid pipe in a metal hydride-phase change material tank. *Appl Therm Eng* 2017;113:554-565.
- [20] Zhang, Y., Wang, J.S., Qiu, J.J., Jin, X., Umair, M.M., Lu, R.W., Zhang, S.F., Tang, B.T. Ag-graphene/PEG composite phase change materials for enhancing solar-thermal energy conversion and storage capacity. *Appl Energy* 2019;237:83-90.
- [21] Karaman, S., Karaipekli, A., Sari, A., Bicer, A. Polyethylene glycol (PEG)/diatomite composite as a novel form-stable phase change material for thermal energy storage. *Sol Energy Mater Sol Cells* 2011;95:1647-1653.
- [22] Song, S.K., Qiu, F., Zhu, W.T., Guo, Y., Zhang, Y., Ju, Y.Y., Feng, R., Liu, Y., Chen, Z., Zhou, J., et al. Polyethylene glycol/halloysite@Ag nanocomposite PCM for thermal energy storage: Simultaneously high latent heat and enhanced thermal conductivity. *Sol Energy Mater Sol Cells* 2019;193:237-245.
- [23] Deng, Y., Li, J., Qian, T., Guan, W., Li, Y., Yin, X. Thermal conductivity enhancement of polyethylene glycol/expanded vermiculite shape-stabilized composite phase change materials with silver nanowire for thermal energy storage. *Chem Eng J* 2016;295:427-435.

- [24] Yang, J., Tang, L.S., Bai, L., Bao, R.Y., Liu, Z.Y., Xie, B.H., Yang, M.B., Yang, W. High-performance composite phase change materials for energy conversion based on macroscopically three-dimensional structural materials. *Mater Horizons* 2019;6:250-273.
- [25] Kholmanov, I., Kim, J., Ou, E., Ruoff, R.S., Shi, L. Continuous Carbon Nanotube-Ultrathin Graphite Hybrid Foams for Increased Thermal Conductivity and Suppressed Subcooling in Composite Phase Change Materials. *ACS Nano* 2015;9:11699-11707.
- [26] Chen, L, Hou, X.S., Song, N., Shi, L.Y., Ding, P. Cellulose/graphene bioplastic for thermal management: Enhanced isotropic thermally conductive property by three-dimensional interconnected graphene aerogel. *Compos Pt A-Appl Sci Manuf* 2018;107:189-196.
- [27] Han, W.F., Ge, C.H., Zhang, R., Ma, Z.Y., Wang, L.X., Zhang, X.D. Boron nitride foam as a polymer alternative in packaging phase change materials: Synthesis, thermal properties and shape stability. *Appl Energy* 2019;238:942-951.
- [28] Kavalenka, M.N., Hopf, A., Schneider, M., Worgull, M., Hölscher, H. Wood-based microhaired superhydrophobic and underwater superoleophobic surfaces for oil/water separation. *RSC Adv* 2014;4:31079-31083.
- [29] Che, W.B., Xiao, Z.F., Wang, Z., Li, J., Wang, H.G., Wang, Y.G., Xie, Y.J. Wood-Based Mesoporous Filter Decorated with Silver Nanoparticles for Water Purification. *ACS Sustain Chem Eng* 2019;7:5134-5141.
- [30] Song, J.W., Chen, C.J., Zhu, S.Z., Zhu, M.W., Dai, J.Q., Ray, U., Li, Y.J., Kuang, Y.D., Li, Y.F., Quispe, N., et al. Processing bulk natural wood into a high-performance structural material. *Nature* 2018;554:224-228.
- [31] Li, T., Song, J.W., Zhao, X.P., Yang, Z., Pastel, G., Xu, S.M., Jia, C., Dai, J.Q., Chen, C.J., Gong, A., et al. Anisotropic, lightweight, strong, and super thermally insulating nanowood with naturally aligned nanocellulose. *Sci Adv* 2018;4(3):eaar37324.
- [32] Song, J.W., Chen, C.J., Yang, Z., Kuang, Y.D., Li, T., Li, Y.J., Huang, H., Kierzewski, I., Liu, B.Y., He, S.M., et al. Highly Compressible, Anisotropic Aerogel with Aligned Cellulose Nanofibers. *ACS Nano* 2018;12:140-147.
- [33] Borrega, M., Ahvenainen, P., Serimaa, R., Gibson, L. Composition and structure of balsa (*Ochroma pyramidale*) wood. *Wood Sci Technol* 2015;49:403-420.

- [34] Fu, Q.L., Ansari, F., Zhou, Q., Berglund, L.A. Wood Nanotechnology for Strong, Mesoporous, and Hydrophobic Biocomposites for Selective Separation of Oil/Water Mixtures. *ACS Nano* 2018;12:2222-2230.
- [35] Guan, H., Cheng, Z.Y., Wang, X.Q. Highly Compressible Wood Sponges with a Spring-like Lamellar Structure as Effective and Reusable Oil Absorbents. *ACS Nano* 2018;12:10365-10373.
- [36] Ma, L.Y., Wang, Q.W., Li, L.P. Delignified wood/capric acid-palmitic acid mixture stable-form phase change material for thermal storage. *Sol Energy Mater Sol Cells* 2019;194:215-221.
- [37] Li, Y., Li, X.J., Liu, D.D., Cheng, X.Y., He, X., Wu, Y.Q., Li, X.G., Huang, Q.T. Fabrication and Properties of Polyethylene Glycol-Modified Wood Composite for Energy Storage and Conversion. *BioResources* 2016;11:7790-7802.
- [38] Zhu, M.W., Song, J.W., Li, T., Gong, A., Wang, Y.B., Dai, J.Q., Yao, Y.G., Luo, W., Henderson, D., Hu, L.B. Highly Anisotropic, Highly Transparent Wood Composites. *Adv Mater* 2016;28:5181-5187.
- [39] Morelli, C.L., Marconcini, J.M., Pereira, F.V., Bretas, R.E.S., Branciforti, M.C. Extraction and Characterization of Cellulose Nanowhiskers from Balsa Wood. *Macromol Symp* 2012;319:191-195.
- [40] Chatterjee, S., Saito, T. Lignin-Derived Advanced Carbon Materials. *ChemSusChem* 2015;8:3941-3958. doi:10.1002/cssc.201500692.
- [41] He, L.H., Wang, H., Yang, F., Zhu, H.Z. Preparation and properties of polyethylene glycol/unsaturated polyester resin/graphene nanoplates composites as form-stable phase change materials. *Thermochim Acta* 2018;665:43-52.
- [42] Chen, Y., Ding, H., Wang, B.F., Shi, Q., Gao, J.K., Cui, Z.X.; Wan, Y.C. Dopamine functionalization for improving crystallization behaviour of polyethylene glycol in shape-stable phase change material with silica fume as the matrix. *J Clean Prod* 2019;208:951-959.
- [43] Safari, A., Saidur, R., Sulaiman, F.A., Xu, Y.; Dong, J. A review on supercooling of Phase Change Materials in thermal energy storage systems. *Renew. Sust Energ Rev.* 2017;70 :905-919.

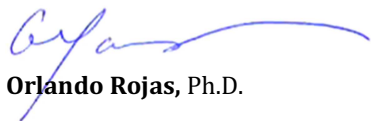
- [44] Ma, L.Y., Guo, C.G., Ou, R.X., Sun, L.C., Wang, Q.W., Li, L.P. Preparation and Characterization of Modified Porous Wood Flour/Lauric-Myristic Acid Eutectic Mixture as a Form-Stable Phase Change Material *Energy Fuels* 2018;132:5453-5461.
- [45] Montanari, C., Li, Y.Y., Chen, H., Yan, M., Berglund, L.A. Transparent Wood for Thermal Energy Storage and Reversible Optical Transmittance. *ACS Appl Mater Interfaces* 2019;11:20465-20472.
- [46] Liang, B., Lu, X., Li, R.P., Tu, W.P., Yang, Z.H., Yuan, T. Solvent-free preparation of bio-based polyethylene glycol/wood flour composites as novel shape-stabilized phase change materials for solar thermal energy storage. *Sol Energy Mater Sol Cells* 2019;200:110037.
- [47] Qu, M., Guo, C., Li, L., Zhang, X. Preparation and investigation on tetradecanol and myristic acid/cellulose form-stable phase change material. *J Therm Anal Calorim* 2017;130:781-790.
- [48] Jiang, L., Liu, Z.M., Yuan, Y., Wang, Y.J., Lei, J.X., Zhou, C.L. Fabrication and characterization of fatty acid/wood-flour composites as novel form-stable phase change materials for thermal energy storage. *Energy Build* 2018;171:88-99.
- [49] Chen, X., Gao, H., Xing, L., Dong, W., Li, A., Cheng, P., Liu, P., Wang, G. Nanoconfinement effects of N-doped hierarchical carbon on thermal behaviors of organic phase change materials. *Energy Storage Mater* 2019;18:280-288.

Highlights

- A form-stable phase change material (FPCM) is prepared from balsa
- Retention of hemicellulose is critical for FPCM performance
- High PCM loading, compressive strength and stability are obtained
- The observed performance of the FPCM is partially explained by PEG affinity with the support
- Reversible thermoregulation is observed for operation at high room temperatures

The authors declare that no conflict of interest.

On behalf of the authors,



Orlando Rojas, Ph.D.

Professor and Canada Excellence Research Chair

Chemical & Biological Engineering | Wood Science | Chemistry

The University of British Columbia, 2360 East Mall (Rm. 259), Vancouver, BC Canada V6T 1Z3

E-mail: orlando.rojas@ubc.ca

www: (CBE) chbe.ubc.ca/ | (Bioproducts Institute) bpi.ubc.ca/

Office: +1-604-822-3457 | Cell: +1-236 558 2682

Declaration of interests

☒ The authors declare that they have no known competing financial interests or personal relationships that could have appeared to influence the work reported in this paper.

☐ The authors declare the following financial interests/personal relationships which may be considered as potential competing interests:

YM, JM, BZ,



Yang Meng, Johanna Majoinen, Bin Zhao, Orlando J. Rojas